Paper 88

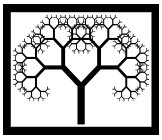

Proceedings of the Eighth International Conference
on Engineering Computational Technology,
B.H.V. Topping, (Editor),
Civil-Comp Press, Stirlingshire, Scotland

A Multilevel Technique based on Nested Local Meshes for Nonlinear Mechanics

L. Barbié[1,2], I. Ramière[1] and F. Lebon[2]
[1] Nuclear Energy Division, Fuel Study Department, Fuel Simulation Laboratory
French Atomic Commission, Saint-Paul-lez-Durance, France
[2] Mechanics and Acoustics Laboratory,
French National Center for Scientific Research, UPR 7051,
Aix-Marseille University, Centrale Marseille, France

Abstract

In this paper an adaptive multilevel mesh refinement method, coupled with the Zienkiewicz and Zhu *a posteriori* error estimator, is applied to solids mechanics with the objective of conducting reliable nonlinear studies in acceptable computational times and memory space. The approach presented in this paper is first validated on linear behaviour, on two and three dimensional simulations. Then nonlinear behaviour is studied. Advantages and limitations of the local defect correction method in solids mechanics problems in terms of error level, CPU time and memory space are discussed. This kind of resolution is also compared with the classical finite element resolution.

Keywords: adaptive mesh refinement, nested local grids, uniform non-data-fitted meshes, local defect correction, a posteriori error estimation, nonlinear solids mechanics, Norton creep, pellet-cladding interaction.

1 Introduction

Adaptive methods are devoted to solve problems with various characteristics length-scale in acceptable computational times and memory space.
In this paper, the test case under study includes local singularities. Moreover, using small elements is more effective to simulate local singularities than increasing the order of the polynomial basis. That is the reason why we decided to use adaptive mesh refinement (AMR) [1] techniques. One of the constraints of the study was to use an existing industrial solver, that means to change only pre-processing and post-processing operations. Thus, we chose to use local multi-grid methods. Furthermore, it induces simple meshes (uniform, structured and regular). As we study elliptic problems discretised by the finite element (FE) method, it is interesting to use structured regular

meshes because it induces well-defined problems. Among the existing local multi-grid methods, the local defect correction (LDC) [2] method was retained because it is not specific to flux conservative problems.
The refinement process is piloted thanks to an a posteriori error estimator based on stress smoothing, called Zienkiewicz and Zhu a posteriori error estimator [3].

2 Adaptive refinement approach

2.1 Local defect correction method

The local defect correction (LDC) method was introduced by Hackbusch [2]. It is based on the multi-grid process [1]. A global coarse grid is used on the whole domain, and only local fine sub-grids are set on areas where more precision is required. Prolongation and restriction operators are defined to link several levels of computation. An example of nested grids is shown on figure 1. The local fine grid lies on a zone of interest defined on the coarse grid. Such type of local sub-grid can be defined recursively until reaching the desired accuracy.

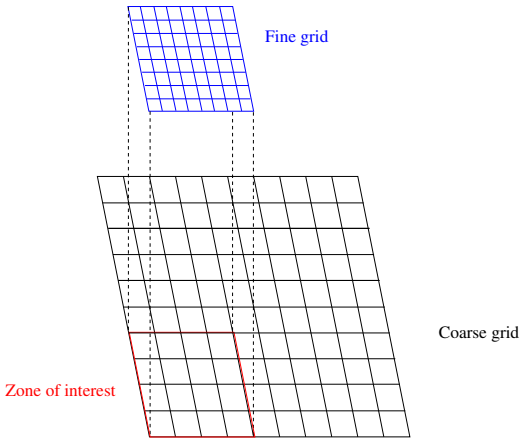

Figure 1: Example of nested meshes used in LDC method

The prolongation operator is used to transport informations from a coarse grid to the next finer one. It consists in defining boundary conditions on the fine grid from the coarse solution.
The restriction operator is defined to transport informations from a fine grid to the next coarser one. It consists in adding a new effort, corresponding to the defect obtained on the coarse problem with the projected fine solution.
Coarse and fine problems are sequentially computed until the solution has converged on the coarser grid. Such an iterative process is traditionally represented by a V-cycle, as on the figure 2.
Let us consider the problem $(\mathcal{P})$ defined on a domain noted Ω of boundary Γ :

$$(\mathcal{P}): \quad \mathcal{L}(u) = f \tag{1}$$

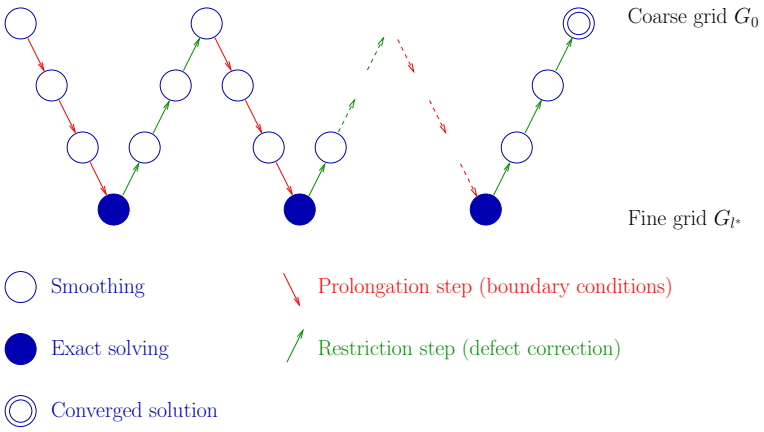

Figure 2: Representation of LDC process : V-cycle

with :

$$\begin{cases} \mathcal{L} & : & \text{usually nonlinear operator} \\ u & : & \text{solution} \\ f & : & \text{right-hand member} \end{cases}$$

A set of nested domains $\Omega_l, 0 \leq l \leq l^*$ with $\Omega_0 = \Omega$ is then defined. Each domain is discretised by a grid G_l of boundary Γ_l. The local problem on iteration k writes :

$$(\mathcal{P}_l^k) : \quad \mathcal{L}_l(u_l^k) = f_l^k \tag{2}$$

with :

$$\mathcal{L}_l = \mathcal{L}_{|G_l}$$

2.1.1 Prolongation step : boundary conditions

In this step, the problem (2) is solved with $f_l^k = f_l^0 \equiv f_{|G_l}$.
On the coarser grid G_0, the boundary conditions of the whole problem is applied since :

$$(\mathcal{L}_0)_{|\Gamma^0} = \mathcal{L}_{|\Gamma} \quad \text{and} \quad (f_0^k)_{|\Gamma^0} = f_{|\Gamma} \quad \forall k \tag{3}$$

The boundary conditions on the other grids $G_l, 1 \leq l \leq l^*$ with $l^* \neq 0$ are represented on figure 3 :

- If $\Gamma_l \cap \Gamma$ is not empty, the boundary conditions of the continuous problem (defined on Γ) are used in the common boundary :

$$(\mathcal{L}_l)_{|\Gamma_l \cap \Gamma} \, (u_l^k)_{|\Gamma_l \cap \Gamma} = (f_l)_{|\Gamma_l \cap \Gamma} \tag{4}$$

- On the other part of the boundary, Dirichlet boundary conditions are applied. A projection operator P_{l-1}^l applied on the next coarser solution u_{l-1}^k enables us to obtain the Dirichlet values :

$$(u_l^k)_{|\Gamma_l \setminus (\Gamma_l \cap \Gamma)} = P_{l-1}^l(u_{l-1}^k) \tag{5}$$

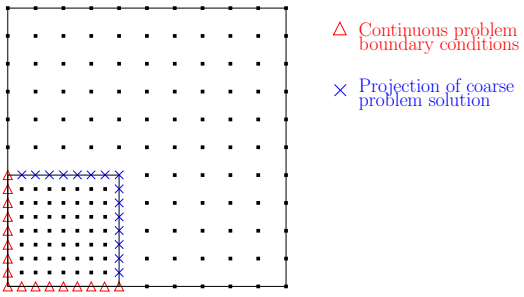

Figure 3: Prolongation step : boundary conditions on G_l ($l \neq 0$)

When the boundary conditions are defined on the fine grid, the discrete problem $(\mathcal{P}_l^k)$ associated to the fine level can be solved.

2.1.2 Restriction step : defect correction

In this section, the boundary conditions defined on the prolongation step are kept to solve the problem $(\mathcal{P}_l^k)$. The restriction step consists in correcting the coarse problem via a defect calculated from the next finer solution.
Two sets of nodes of G_l have to be defined, see figure 4. A_l contains the nodes of the coarse grid G_l strictly included on the domain discretised by G_{l+1}. $\mathring{A}_l$ is made up of the interior nodes of A_l (in the sense of the discretisation scheme).

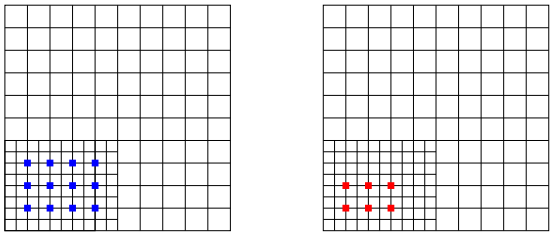

Figure 4: Restriction zone A_l on the left and correction zone $\mathring{A}_l$ on the right (e.g. for operator Δ)

The solution obtained on the fine grid G_{l+1} is restricted to the nodes of A_l :

$$\tilde{u}_l^k(x) = (R_{l+1}^l u_{l+1}^k)(x) \quad \forall x \in A_l \tag{6}$$

where R_{l+1}^l is the polynomial interpolation from fine grid G_{l+1} to the coarse grid G_l.
The local defect associated to this solution is computed on the nodes of $\mathring{A}_l$:

$$r_l^k(u)(x) = (\mathcal{L}_l(\tilde{u}_l^k) - f_l^0)(x) \quad \forall x \in \mathring{A}_l \tag{7}$$

Then the coarse solution u_l is corrected by solving the coarse problem with the modified right-hand member :

$$f_l^k = f_l^0 + \chi_{\mathring{A}_l} r_l^k(u) \tag{8}$$

where $\chi_{\mathring{A}_l}$ is the characteristic function of $\mathring{A}_l$.

2.2 Zienkiewicz and Zhu a posteriori error estimator

In order to define automatically the zone of interest, an a posteriori error estimator is used. This kind of estimator is devoted to estimate a measurement of the discretisation error. The Zienkiewicz and Zhu (ZZ) [3, 4, 5] a posteriori error estimator was selected because it is not time consuming and it is easy to apply.

Almost all the a posteriori error estimators developed for solids mechanics are based on the fact that the classical FE resolution does not verify the continuity of the stress field. The ZZ a posteriori error estimator consists in constructing a stress solution σ^* more regular than the FE one σ_h. The local estimator $\eta_{E,h}$ on an element E is defined as :

$$\eta_{E,h} = \|(\sigma_h^*)_E - (\sigma_h)_E\| \tag{9}$$

The element value is obtained from nodes values. The values of the FE stress σ_h at the discretisation nodes are obtained by interpolating the values at the Gauss points. To obtain the estimated stress σ_h^*, two methods are proposed by Zienkiewicz and Zhu :

- The simplest and cheapest one [3] consists in averaging the value of the FE stress σ_h on the elements surrounding the node. However, its is not very efficient for very coarse grids or for high-order elements.
- The second one, called "super convergent patch recovery" [4, 5], is based on patch, which is the union of several elements. On each patch, a high-order polynomial function is defined, which minimises the root mean square gap with respect to σ_h on "super convergent" points (Gauss points in one dimensional problems). Then an average of each patch contribution is made to obtain σ_h^*. This method is more expensive but leads to better approximations.

3 Test case

The pellet-cladding interaction (PCI) [6] appears during irradiation in pressurised water reactors, which are the essential of french nuclear reactors.
The fuel is formed of cylindrical pellets of 8.2 mm diameter, composed of uranium dioxide (UO_2), piled up in a zircaloy cladding. During irradiation, two phenomena lead to PCI :

- The fuel pellet quickly cracks (see on figure 9 left). Moreover, the fuel pellet swells and the cladding creeps due to external pressure, that induces contact between the pellet and the cladding. The pellet cracking results in discontinuous contact.
- An other phenomenon, illustrated by figure 5 adds discontinuities. As the fuel pellet has a finite axial size, the temperature gradient leads to a hourglass shape deformation of the pellet. Thus, the contact between the fuel and the pellet

appears first in front of the inter-pellet plane, then it develops towards the mid-pellet plane. The hourglass shape phenomenon results in a concentration of stresses around the inter-pellet plane.

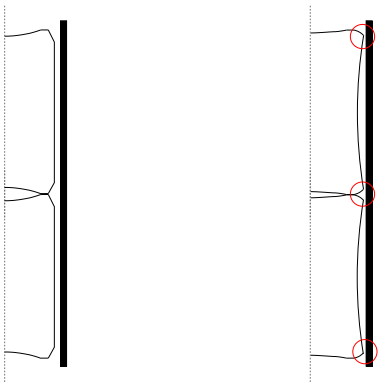

Figure 5: Illustration of the hourglass shape phenomenon : before (left) and after (right) irradiation

Modelling precisely the PCI is of great importance, as it concerns the integrity of the cladding which is the first confinement barrier for the irradiated fuel. That is why research and development on this item are still undertaken worldwide in order to improve the understanding of the mechanisms possibly leading to PCI failure, as well as to qualify a PCI resistant rod design. Complete 3D simulations are currently limited because of the required unstructured and irregular mesh, inducing an ill-conditioned system with an important number of degrees of freedom. The LDC method seems then well suited for this kind of application. However, this method has stood the test of time in fluid mechanics but is almost unused in other fields of physics. For this reason, the use of LDC method will be first validated on linear structural mechanics.

In all this study, a simplified PCI model is used. We are only interested in the cladding response, and the contact with the pellet is represented by a discontinuous pressure on the internal radius of the cladding. The validation step, see part 4, will consist in supposing a linear elastic behaviour of the cladding. Then, the LDC method will be extended to nonlinear behaviour on section 5.

As there is generally no analytical solution to our test cases, we use reference solutions obtained by solving the test problems on really fine meshes, using a classical resolution with the Q_1 FE method.

4 Validation study

The two phenomena characteristics of PCI are first modelled separately in 2 two-dimensional studies then they are gathered in the three-dimensional study.

4.1 Hourglass shape phenomenon

4.1.1 Problem definition

The first model is axisymmetric and represents the hourglass shape phenomenon. The first advantage of this method is that the geometry is very simple, as the domain studied is a rectangle. So regular structured uniform meshes perfectly representing the real geometry can be used.
The hourglass shape is represented by a peak of pressure around the inter-pellet plane. Thanks to symmetrical conditions, only half of the pellet is simulated. On figure 6, the geometry of the problem and the boundary conditions are available.

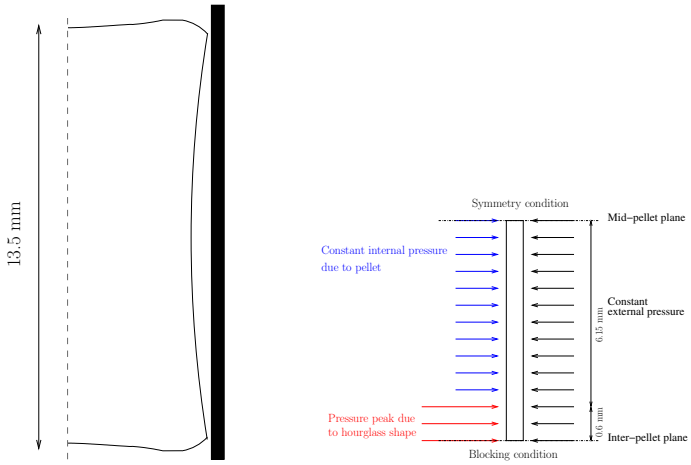

Figure 6: Problem definition - 2D axisymmetric model

4.1.2 Results

On figure 7, an example of nested meshes used for our simulation can be seen. The current mesh is in black and the zone of interest is in green. This refinement zone is obtained selecting the elements $L \subset \Omega_l$ that respect :

$$e_L > \alpha(\max_{K \subset \Omega_l} e_K - \min_{K \subset \Omega_l} e_K) \tag{10}$$

where e_L is the local ZZ error. In this study, we set $\alpha = 0.2$. In order to obtain nested structured cartesian meshes, some elements have to be added to the selected ones. Indeed, working with cartesian grids permits to avoid numerical artifacts due to reflex corners and to increase the speed of the solver.
The reference solution was obtained on a uniform mesh of space step $5.10^{-3}mm$ in each direction.
We study the L_2 error between this reference solution and the solution obtained after convergence on the global coarse grid using the LDC method. This error is plotted on figure 8 according to the distance between the real singularity and the approximated

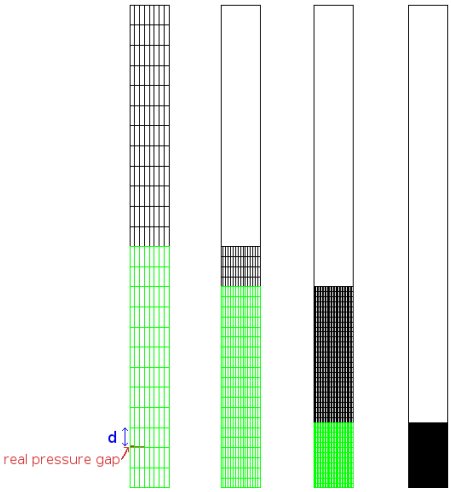

Figure 7: Example of nested structured meshes generated automatically thanks to a posteriori error estimator - 2D axisymmetric model

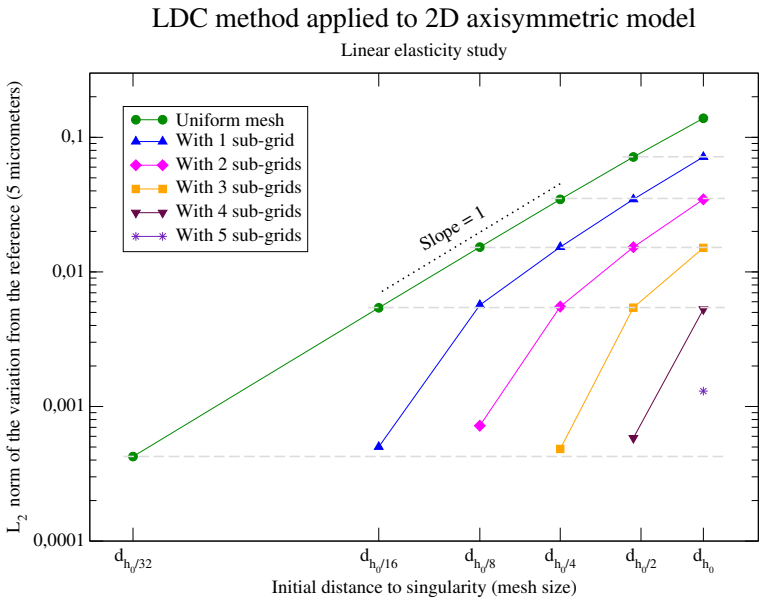

Figure 8: L_2 error according to the mesh - 2D axisymmetric model

one on the initial coarse mesh (see on figure 7), and to the number of sub-grids.
The first conclusion to be drawn is that the method converges at the first-order with respect to the initial distance to the singularity. The lost of one order of convergence compared to the classical Q_1 FE resolution was expected since the singularity has been approximated, as mentioned by Ramière [7]. The second conclusion is that the LDC method conserves the order of convergence with respect to the local finest distance to the singularity. Indeed the same error level is obtained with a local refinement as with a global one with a discretisation step equal to the local finest one. Thus, the LDC method converges as $O(d_{h_{fine}})$, where $d_{h_{fine}}$ corresponds to the local distance

to the singularity. This conclusion remains still true even for an important number of sub-grids or an important decrease of the error.

This test case validates the use of the LDC method for linear elasticity, and the use of Zienkiewicz and Zhu a posteriori error estimator to detect refinement zones.

4.2 Pellet cracking phenomenon

4.2.1 Problem definition

The second model represents the pellet cracking and verifies the plane strain hypothesis. As the geometry is curved, the meshes will be regular structured but non uniforms, only "quasi uniforms". The goal is to validate the LDC method on a less classical case, particularly when the geometry has to be approximated. Indeed, the meshes generation implies that the approximation of the curvature remains the initial coarser one on all the sub-grids.
The cracking phenomenon is represented by a pressure discontinuity on the internal radius of the cladding, in front of the crack opening. The pellet is assumed to crack in a regular way, see [8]. Using symmetrical conditions, only $1/16$ of the pellet is represented. On the figure 9, the geometry of the problem and the boundary conditions are available.

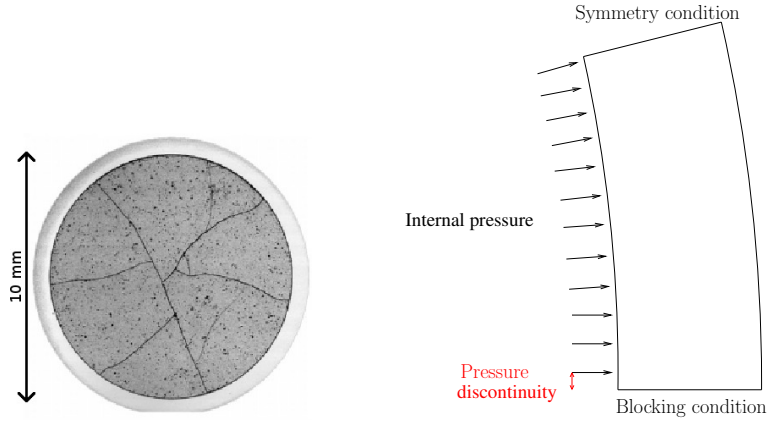

Figure 9: Problem definition - 2D plane strain model

4.2.2 Results

We use the same method as in the hourglass case to obtain nested meshes, of which an example is plotted on figure 10. We can notice here that the refinement zone is very localised. Moreover, if this refinement zone is compared to an example of crack observed in a cladding after irradiation (see figure 11), we can observe that the refinement zone is in good coherence with the failure position.

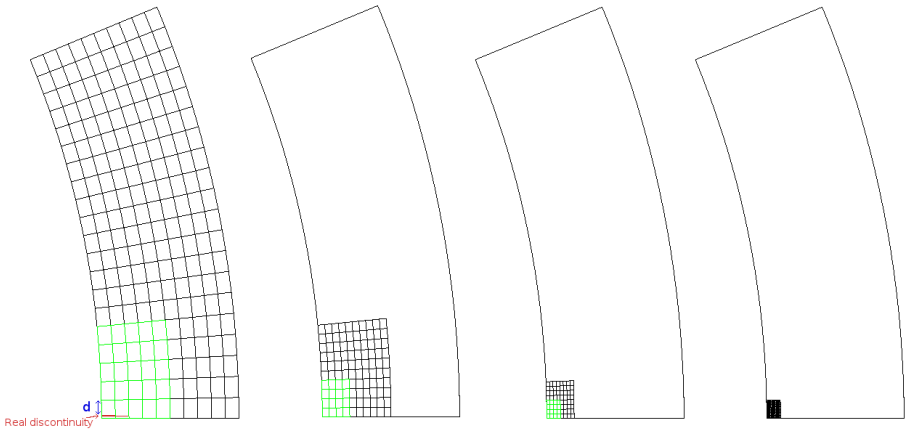

Figure 10: Example of nested structured meshes generated automatically thanks to a posteriori error estimator - 2D plane strain model

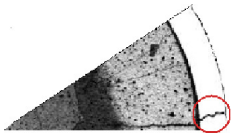

Figure 11: Example of crack observed on a cladding after irradiation

In this case, to validate our approach, we could use the analytical solution developed by Roberts [9]. However this solution is written with a Fourier decomposition, and we cannot perform the number of terms required to obtain an enough precise solution. So, as in the previous case, we use a reference solution obtained on a really fine mesh ($1.10^{-3}mm$ in each direction) with a classical FE resolution.
The L_2 error between this reference solution and the LDC solution is plotted on figure 12 according to the initial distance between the real singularity and the approximated one, and to the number of sub-grids.
This study leads to the same conclusions than the previous one. Without local refinement, the approximation of singularity induces a convergence in $O(d_h)$. Moreover, we find again the convergence as $O(d_{h_{fine}})$ for the local multi-grid method. The observed stagnation is due to the fact that $d_{h_0/32} = d_{h_0/16}$.
Finally, even for small error ($< 1.10^{-3}$), the error due to geometry approximation (the approximation of the curvature remains the initial coarser one on all the sub-grids) seems negligible compared to the error due to singularity approximation.

To optimise the ratio precision obtained over CPU time, the figure 13 represents the L_2 error with respect to CPU time and to the number of sub-grids.
From this figure, we can conclude that the more the precision expected is constraining, the more the use of an initial coarse mesh with many sub-grids is advantageous.

In addition, the LDC method is classically used with a refinement ratio of 2. As

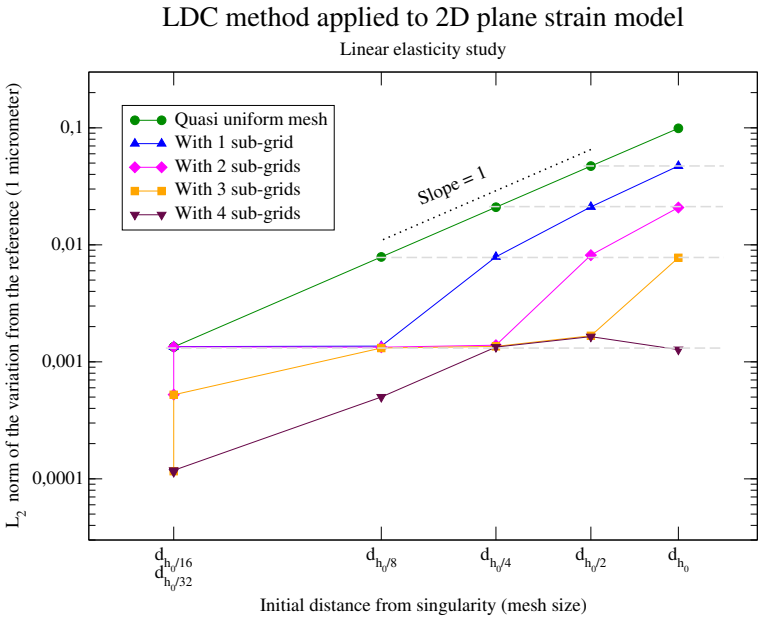

Figure 12: L_2 error according to the mesh - 2D plane strain model

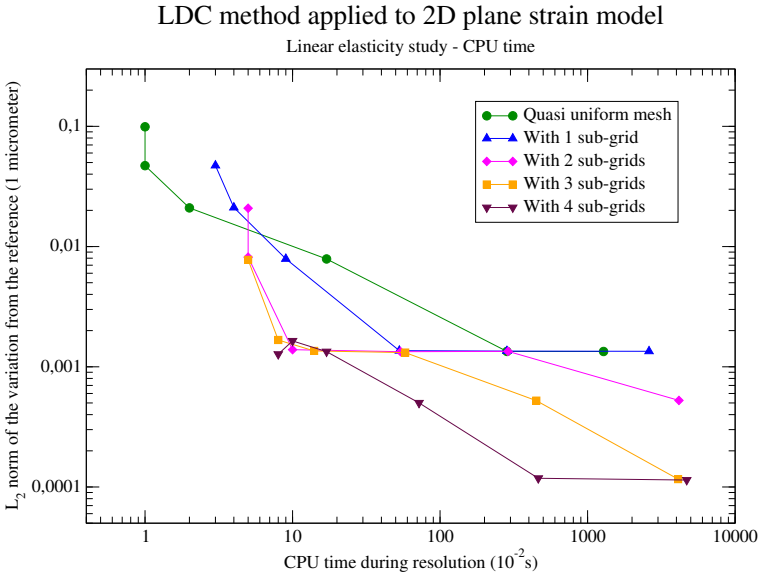

Figure 13: CPU time according to L_2 error - 2D plane strain model

there is no theoretical limitation for the choice of the refinement ratio, we decided to study the performance of the LDC method with a refinement ratio of 4. The convergence results are presented on figure 14.
As expected, we obtain the same error levels for simulations made with two successive refinements of ratio 2 than with one refinement of ratio 4, even for small errors. Thus, the convergence as $O(d_{h_{fine}})$ is conserved, whatever the refinement ratio used. The CPU time and space memory will be compared in the next section.

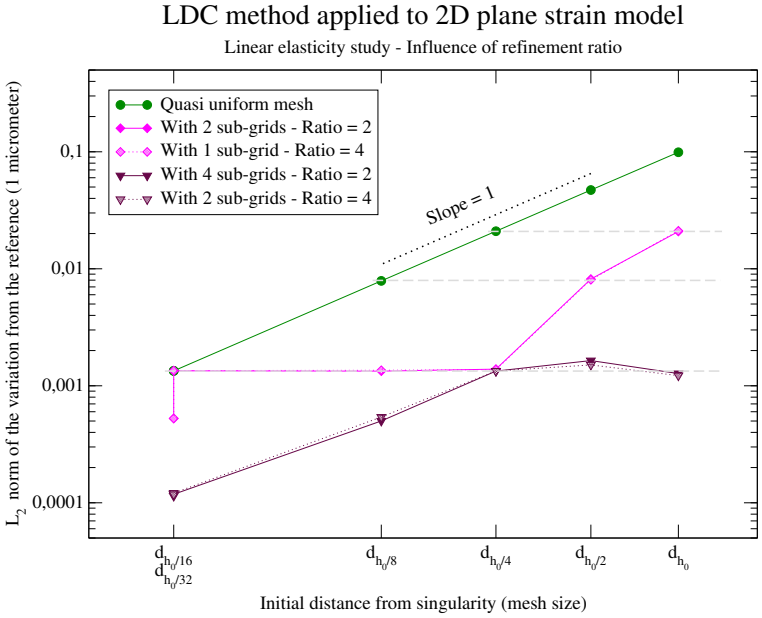

Figure 14: Influence of refinement ratio - 2D plane strain model

4.2.3 Comparison with classical FE solver

According to the previous conclusions made on figure 13, it seems more attractive to use a very coarse initial mesh and a lot of sub-grids. Moreover, the use of refinement ratio of 4 seems to be attractive, according to results on figure 14. That is why we decided to use for our LDC method an initial mesh of size $h_0/2$, with 1 to 7 sub-grids (if refinement ratio is 2) or 1 to 4 sub-grids (if the refinement ration is 4). We also tried a variable refinement ratio, equal to 2 or 4 according to the number of elements on the refinement zone. Classical resolution is made on meshes refined locally around the singularity. The meshes on figure 15 are examples of meshes used for this comparison, and the CPU time are reported on figure 16.
The first conclusion to be drawn is that in this case, using a refinement ratio of 4 instead of 2 is not so attractive in terms of CPU time. Nevertheless, this conclusion is strongly related to the size of the zone of interest. Indeed, the use of a larger ratio allows to limit the number of sub-grids, but may imply the use of more extended grids and thus more nodes than necessary in some zones (in our case, there are approximately twice more elements for the same error).

The use of a variable refinement ratio, equal to 2 or 4 according to the levels, is also possible thanks to the LDC algorithm. It seems attractive, specially in terms of computational time because it accelerates the speed of convergence compared to the refinement ratio of 2 (number of V-cycles) and contains less nodes than refinement ratio of 4. In this case, we observe this good compromise because it is the best curve according to computational time on figure 16, and the total number of elements included between those obtained with a refinement ratio of 2 or of 4. However, it seems

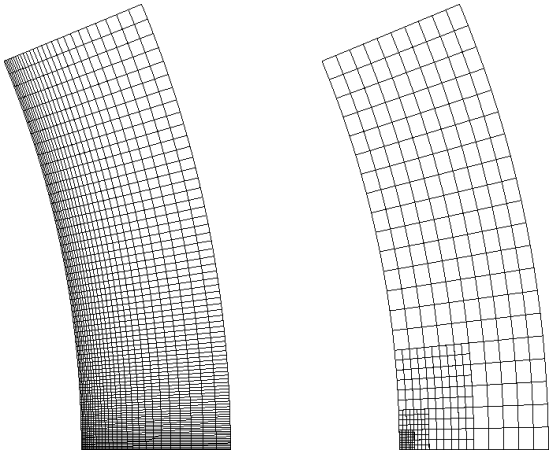

Figure 15: Examples of meshes used in the comparison study : classical mesh (left) and LDC mesh with 3 sub-grids and refinement ratio of 2 (right)

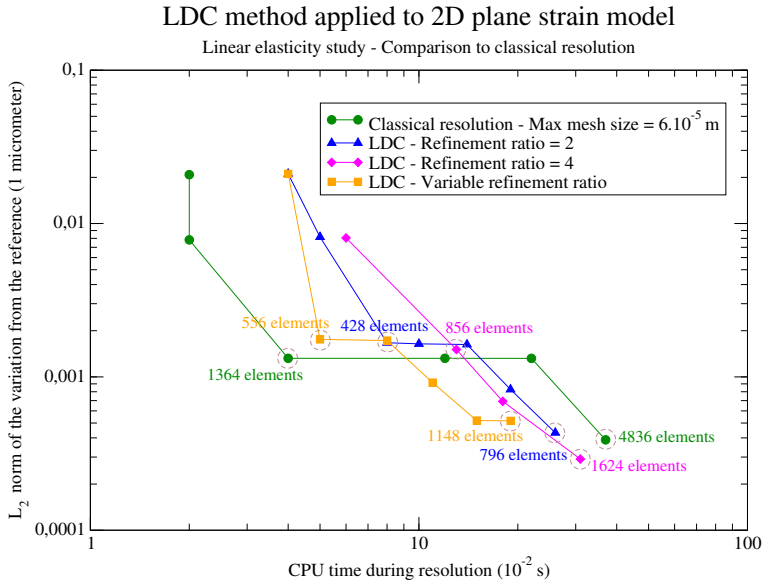

Figure 16: CPU time and mesh size according to L_2 error - 2D plane strain model - Comparison between LDC solver and classical FE solver

difficult to find a non heuristic criterion to choose the refinement ratio on each level.

In addition, we compare CPU times of a classical FE resolution and of a LDC one. We can notice that the LDC solver is efficient. Indeed, equivalent computational times are obtained for equivalent levels of error. For errors about 1.10^{-3}, computational times are approximately twice larger for the LDC method, but these times remain very small ($\sim 5.10^{-2}s$). For smaller errors, about 1.10^{-4}, the CPU time required for the LDC resolution is twice smaller than the on required for a classical FE resolution. Moreover, this case is particularly unfavourable for the LDC method, because the studied problem is simple (two-dimensional, in linear elasticity) and then

quickly well solved by the classical FE solver. The fact to reach the same efficiency than the classical FE solver for this simple test problem is hence very satisfying.

Moreover, our method does not require preliminary study in order to obtain a mesh refinement adapted to the problem. As the generation of the sub-grids is automatic, only a mesh size for the coarse level and a refinement criterion are necessary. The use of the LDC method thus makes possible to save preprocessing times, that can be really important, especially in 3D.

Lastly, from a memory space saving point of view, the LDC method is also attractive. Indeed, even if extra informations are stored (boundary conditions on the levels, reversed matrices of rigidity, right-hand member,...), each local grid is much smaller than an equivalent global refined grid. In particular the total number of elements of all the sub-grids is far smaller than the number of elements of the locally adapted grid used currently (4 times less elements for an error about 1.10^{-3} and 6 times less for an error about 1.10^{-4}, see figure 16).

To conclude, the LDC solver seems very attractive. Indeed, even for a simple test case which is a priori unfavourable for the LDC solver, we obtain for a given error an equivalent CPU time and much less elements. This results give confidence in the use of the LDC solver for more complex studies.

4.3 Three-dimensional phenomena

4.3.1 Problem definition

This model gathers the two previous phenomena on a three-dimensional geometry. The goals are multiples : validate our approach on a three-dimensional case, validate detection and treatment of several singularities of different characteristic length-scale and verify the LDC method performances.
We have to notice that, due to the size of the problem under study, we cannot obtain an accurate reference solution with an uniform mesh any more. The reference solution is hence obtained with a mesh of space-step varying from 10 to 100 μm.

We use the same method as in sections 4.1 and 4.2 to obtain nested meshes. A preliminary study showed that the refinement criterion has to be modified in order to well detect the two singularities. The criterion α is set to 0.15 for the first refinement level, to select accurately the two singularities. The value $\alpha = 0.2$ can be kept on other levels. Indeed, the ZZ a posteriori error estimator has difficulty to accurately detect two singularities if their characteristic sizes are different. However, modifying this criterion induces a refinement zone too large for one of the singularity. This is a limitation of the ZZ a posteriori error estimator.
The L_2 error between the reference solution and the LDC solution is plotted on figure

17 according to the initial distance between the real position of the intersection of the two singularities and the approximated one, and to the number of sub-grids.

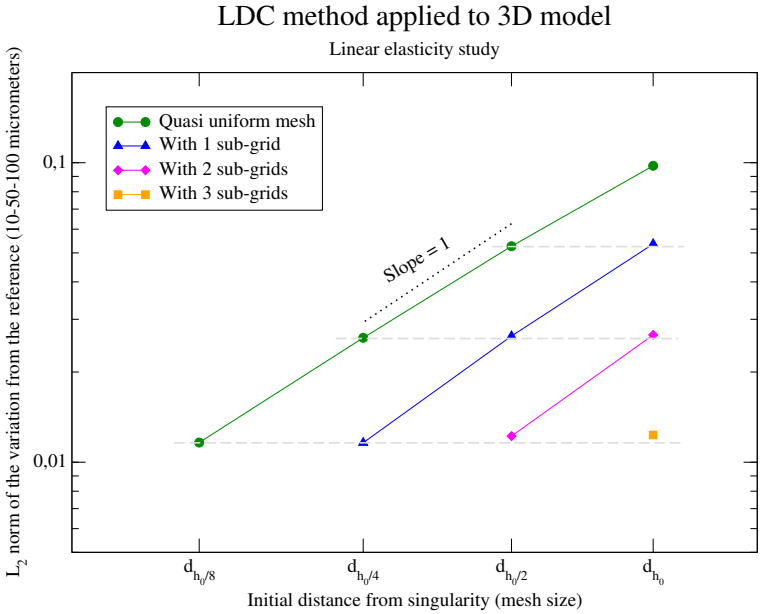

Figure 17: L_2 error according to the mesh - 3D model

The expected first-order convergence is reached. Moreover, the error improvement due to the refinement strategy remains true in a three-dimensional context, as the method still converges as $O(d_{h_{fine}})$.

The study of the CPU time required with respect to the number of sub-grids (see figure 18) leads to the same conclusions as for two-dimensional cases. The more the solution is aimed to be precise, the more the use of an initial coarse mesh and several local sub-grids improves the ratio of the obtained precision over CPU time. The CPU time is for example reduced of a factor 30 between a simulation with an initial mesh step of $h_0/8$ and $l^* = 0$ and a global mesh step of $h_0/2$ and $l^* = 2$.

4.3.2 Comparison with classical FE solver

A comparison between the adaptive refinement method and a classical FE resolution was also made for the three-dimensional case. As the reference solution is not very accurate, we only compare two simulations, for a quasi equivalent local fine mesh size. The results are presented in detail in table 1. These results are really encouraging. Indeed, the ratio error over local fine mesh size seems to be the same. Moreover, it should be noted that for the LDC method, the number of elements represents the total number on all the grids. Thus all these elements are never treated at the same time, which explains the significant acceleration of the computational time ($\div 5$).
Lastly, it must be noticed that, due to the limitation of ZZ a posteriori error estimator

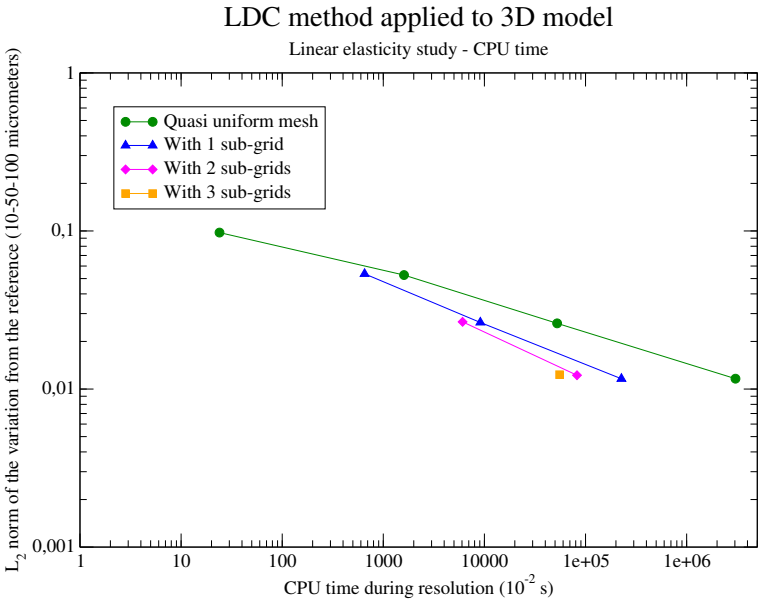

Figure 18: CPU time according to L_2 error - 3D model

Mesh	L_2 error	CPU time	Number of elements
Classical resolution 65 to 103 μm	$1.02\ 10^{-2}$	$24.10\ 10^{2}\ s$	105196
LDC h_0, 3 sub-grids local h_{fine} 79 μm	$1.23\ 10^{-2}$	$5.53\ 10^{2}\ s$	77744

Table 1: Comparison between LDC and classical resolution - 3D model

for the treatment of two singularities, the refined meshes obtained are not efficiently localised.

5 Nonlinear study : Norton creep behaviour

As the LDC process for solids mechanics has been validated for linear elastic behaviour in previous section, we will now complex the cladding behaviour. A Norton creep behaviour, which is nonlinear, is now studied. It adds to the linear behaviour a nonlinear strain which is defined as :

$$\dot{\varepsilon}^{vp} = \left(\frac{\sigma}{K}\right)^n \tag{11}$$

where K and n are two given coefficients.
The main difficulty in this case is linked to the stresses evaluation to compute the defect. This is not commonplace to obtain analytically the stresses from the displacements, as in linear study. In the other hand, a reliable projection method of the stresses does not exist. That is why we choose restrict the displacements, then to solve a new

nonlinear problem with this restricted displacement imposed in order to obtain the restricted stresses, which allows us to compute the defect.

The test case under study is the two-dimensional pellet cracking phenomenon. The same method as for the linear study was applied to obtain the refinement zones. On the example of nested meshes on figure 19, it must be noticed that the refinement areas (in green) are quite larger than in linear context (see on figure 10).

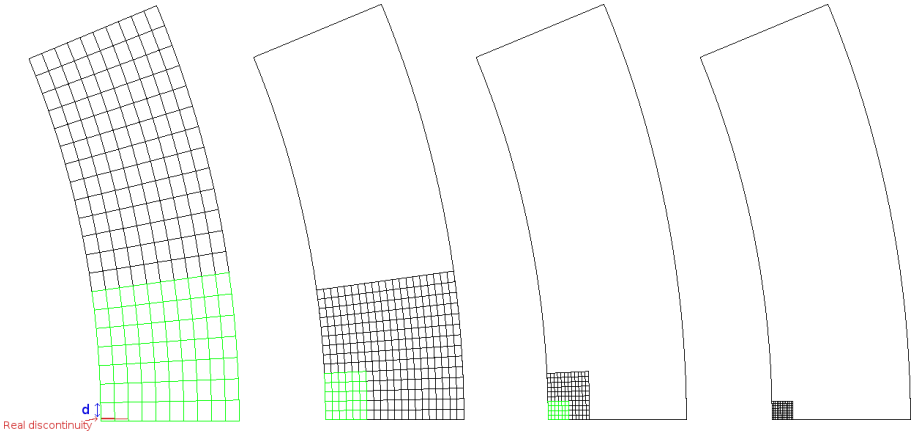

Figure 19: Example of nested structured meshes generated automatically thanks to a posteriori error estimator - 2D plane strain model - Norton creep behaviour

On figure 20, the L_2 error between the reference solution (obtained with an uniform regular structured mesh of size $5.10^{-3}mm$) and the nonlinear LDC solution is plotted according to the initial distance from the singularity and the number of sub-grids.
The nonlinear behaviour does not deteriorate the theoretical convergence in $O(d_{h_{fine}})$ of the LDC method obtained on linear study. This is very encouraging as we should also be attractive in terms of number of elements and CPU time, as in the linear study.

A comparison between the LDC solver and the classical FE solver has been also started for the nonlinear behaviour. The first comparison was made on Von Mises field on the cladding, see figure 21.
The stress distributions obtained using the classical FE resolution and the LDC method are equivalent. Moreover, the maximal relative error is about 1%, which is really interesting according to the current precision of the physical models.
In table 2, we compare the two simulations, for a quasi equivalent local fine mesh sizes.
The LDC method is very attractive in terms of number of elements, as 6 times less elements are necessary to obtain a quasi equivalent precision. On the other hand, the ratio error over CPU time seems to be equivalent, which is far from the results expected following the linear study (see figure 16). However, we do not use efficiently the LDC method. In particular, a significant acceleration of the computational time could be obtain by using the previous computed solutions in the LDC cycles. It seems

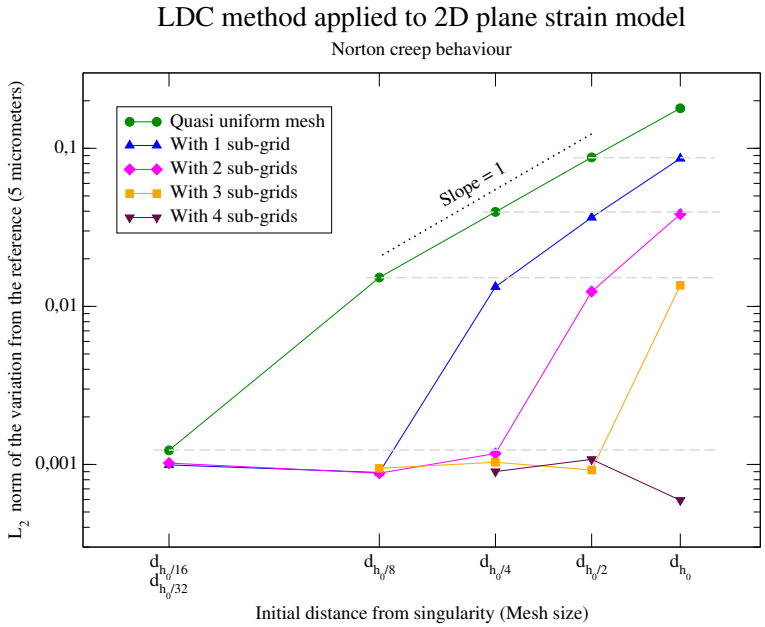

Figure 20: L_2 error according to the mesh - 2D plane strain model - Norton creep behaviour

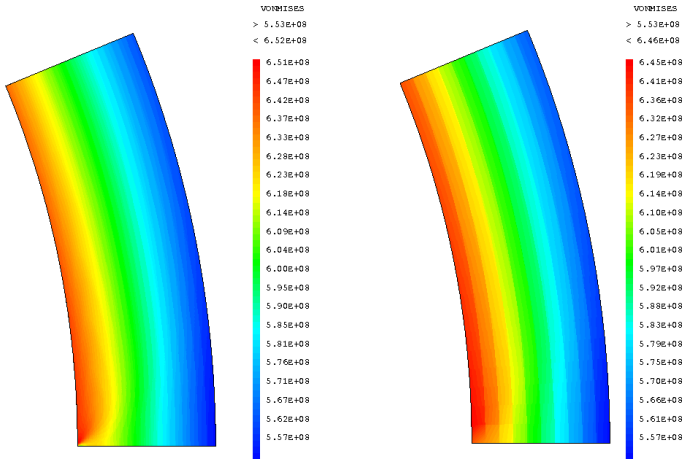

Figure 21: Von Mises field for the classical FE resolution (left) and for the LDC one (right) - 2D plane strain model - Norton creep behaviour

Mesh	L_2 error	CPU time	Number of elements
Classical resolution 7.1 to 56.6 μm	$9.86\ 10^{-4}$	$2.69\ 10^2\ s$	3708
LDC $h_0/2$, 3 sub-grids local h_{fine} 12.8 μm	$9.22\ 10^{-4}$	$3.19\ 10^2\ s$	680

Table 2: Comparison between LDC and classical resolution - 2D(r,θ) nonlinear model

surprising that for a coarser local mesh-step, the LDC method leads to a better pre-

cision. this has to be studied furthermore, but the first conclusion to be drawn from these results is that the nonlinear simulations are sensitive to the regularity of the mesh.

This test case is a first validation step in the use of the LDC method and the use of Zienkiewicz and Zhu a posteriori error estimator to detect refinement zones for nonlinear mechanical behaviour.

6 Conclusion

The local defect correction (LDC) method, which is an adaptive mesh refinement (AMR) method based on multilevel resolutions, has been applied to a simplified problem stemming from the pellet-cladding interaction in pressurised water reactors. We focused only on the cladding response subject to discontinuous pressures from the fuel pellet.
Firstly, we focus on a linear behaviour. This first step is necessary to validate this method and study its potentially in structural mechanics, in a problem with so strong local singularities. The local sub-grids are automatically generated using the Zienkiewicz and Zhu (ZZ) a posteriori error estimator.
The first results obtained for the 2 two-dimensional studies are very satisfying. The expected theoretical convergence as $O(d_{h_{fine}})$ is obtained, where $d_{h_{fine}}$ is the distance between the real singularity and its approximation on the finest grid which mesh size h_{fine}. Saving of computational time and memory space is thus very large in comparison with a classical resolution by the finite element method.
The LDC method is also well adapted for three-dimensional studies, but the ZZ a posteriori error estimator has trouble to efficiently detect two singularities of characteristic sizes to different, which leads to a too large refinement zone.
To conclude, the first results obtained in a nonlinear context give confidence in using the LDC method in complex studies. The linear results are confirmed by the nonlinear study, and the same order of convergence is obtained.

The prospects of this study is first to couple the LDC method with a domain decomposition method in order to be able to treat efficiently several singularities of different characteristic length-scale using the Zienkiewicz and Zhu a posteriori error estimator. In the same time, the nonlinear study will be completed.
Then, a temporal variation will be added to treat the temporal evolution of grids position and size.
Lastly, the contact with the pellet will be modelled. The main difficulty will then consist in treating two grids facing each other in a LDC context.

References

[1] A. Brandt, "Multi-level adaptive solutions to boundary-value problems", *Mathematics of Computation*, 31: 333–390, 1977.

[2] W. Hackbusch, "Local Defect Correction Method and Domain Decomposition Techniques", *Computing Suppl. Springer-Verlag*, 5: 89–113, 1984.

[3] O. Zienkiewicz, J. Zhu, "A simple error estimator and adaptive procedure for practical engineering analysis", *International Journal for Numerical Methods in Engineering*, 24: 337–357, 1987.

[4] O. Zienkiewicz, J. Zhu, "The superconvergent patch recovery and a posteriori error estimation. Part I: The recovery technique", *International Journal for Numerical Methods in Engineering*, 33: 1331–1364, 1992.

[5] O. Zienkiewicz, J. Zhu, "The superconvergent patch recovery and a posteriori error estimation. Part II: Error estimates and adaptivity", *International Journal for Numerical Methods in Engineering*, 33: 1365–1382, 1992.

[6] B. Michel, J. Sercombe, G. Thouvenin, R. Chatelet, "3D fuel cracking modelling in pellet cladding mechanical interaction", *Engineering Fracture Mechanics*, 75: 3581–3598, 2008.

[7] I. Ramière, "Convergence analysis of the Q_1-finite element method for elliptic problems with non-boundary-fitted meshes", *International Journal for Numerical Methods in Engineering*, 75(9): 1007–1052, 2008.

[8] C. Nonon, S. Lansiart, C. Struzik, D. Plancq, S. Martin, G. Decroix, O. Rambouille, S. Beguin, B. Julien, "Differential PCI behaviour of PWR fuel rods under transient conditions", in *International Topical Meeting on LWR Fuel Performance*, 2004.

[9] G. Roberts, "The concentration of stress in cladding produced by the expansion of cracked fuel pellets", *Nuclear Engineering and Design*, 47: 257–266, 1978.